Fine structure of proton-neutron mixed symmetry states in some $N = 80$ isotones

N. Lo Iudice,[1,*] Ch. Stoyanov,[2,†] and D. Tarpanov[2,‡]

[1]*Dipartimento di Scienze Fisiche, Universitá di Napoli "Federico II" and Istituto Nazionale di Fisica Nucleare, Monte S Angelo, Via Cintia I-80126 Napoli, Italy*

[2]*Institute for Nuclear Research and Nuclear Energy, Bulgarian Academy of Sciences, 1784 Sofia, Bulgaria*

(Received 25 January 2008; published 15 April 2008)

A microscopic multiphonon approach is adopted to investigate the structure of some low-lying states observed experimentally in the $N = 80$ isotones ^{134}Xe, ^{136}Ba, and ^{138}Ce. The calculation yields levels and electromagnetic transition strengths in good agreement with experiments and relates the observed selection rules to the neutron-proton symmetry and phonon content of the observed states. Moreover, it ascribes the splitting of the $M1$ strength in ^{138}Ce to the proton subshell closure which magnifies the role of pairing in the excitation mechanism.

DOI: 10.1103/PhysRevC.77.044310 PACS number(s): 21.10.Re, 21.60.Ev, 23.20.−g, 27.60.+j

I. INTRODUCTION

Low-energy spectra in nuclei are of crucial importance for understanding the correlations among valence nucleons. They include elementary excitations, like the low-lying 2^+ quadrupole mode, but also complex excitations to be described by *multiphonon* states.

In the neutron-proton (np) interacting boson model (IBM-2) [1], these multiphonon states are classified according to the quantum number F-spin. The states with maximum F-spin ($F = F_{\max}$) are fully symmetric with respect to the exchange of proton and neutron bosons. The states with $F = F_{\max} - 1$ have a np mixed symmetry (MS) [2–4]. The IBM-2 provides a specific signature for states of a given np symmetry. Strong $E2$ transitions connect the states with the same F-spin differing by one d boson, while states having the same number of bosons and different F-spin are coupled by strong $M1$ transitions.

While the experimental evidence of the np symmetric excitations was well established for all nuclei long ago [5], only in the 1980's was the first MS state, the well-known scissors mode [6], observed in deformed nuclei in a high resolution inelastic electron scattering experiment [7]. Since then, the mode was identified in most deformed nuclei and thoroughly analyzed experimentally [8,9] and theoretically [10].

The scissors mode in deformed nuclei was for several years the only MS excitation observed experimentally. Only recently, the existence of MS states in spherical nuclei was established experimentally [11]. They were identified unambiguously for the first time in ^{54}Cr [12] and ^{56}Fe [13]. More massive evidence was gained through an experiment on ^{94}Mo [14]. Since then, other experiments have produced more data for the same nucleus [15–18] and have provided evidence of new MS states in a series of nuclei near the neutron magic number $N = 50$ [19–27]. Few other experiments have established the existence of MS states also in the region around $N = 82$ [28–31].

In most nuclei explored experimentally, the measured levels and transition probabilities fit well in the IBM-2 scheme which classifies the states according to the F-spin and the number of bosons. These low-lying states have also been investigated theoretically within microscopic approaches. A shell model (SM) calculation, performed within a severely truncated space, has accounted for several properties of MS states [20,32]. A more thorough investigation was performed within the quasiparticle-phonon model (QPM) [33–36].

The QPM, developed by Soloviev and coworkers [37], consists of constructing a multiphonon basis out of phonons generated in quasiparticle-random-phase approximation (QRPA). Such a basis is then used to diagonalize a Hamiltonian of general separable form. The basis constructed covers a very large configuration space and, because of its phonon structure, is naturally related to semiclassical models and algebraic approaches as the IBM. In fact, the QPM multiphonon basis states can be viewed as the microscopic counterparts of the IBM bosonic states.

Because of such a close link, the QPM can provide a microscopic support to the IBM scheme. Indeed, QPM calculations have confirmed the IBM classification of the observed states according to their phonon structure and their np symmetry as well as the IBM selection rules which provide the signatures for these low-lying states [33,34].

On the other hand, the QPM can give important additional information. Indeed, it discloses the shell structure of these states and, due to its many degrees of freedom, including spin, can describe properties which are outside the domain of IBM.

The theoretical investigations have been confined so far to the $N = 50$ region. Apart from a QPM digression on ^{136}Ba, the region around $N = 82$ has been little explored. On the other hand, investigating those nuclei is of considerable interest not only for their intrinsic value, but also since recent experiments [29] have shown that the nuclear properties in this region do not change smoothly with the number of valence protons, suggesting important shell effects. Hence, the necessity of microscopic studies. This is carried here in QPM following the route undertaken in previous investigations [33–36].

II. A VERY BRIEF OUTLINE OF THE PROCEDURE

In the QPM procedure one assumes a Hamiltonian composed of a Woods-Saxon one-body piece and a two-body potential which is the sum of several multipole-multipole

*loiudice@na.infn.it
†stoyanov@inrne.bas.bg
‡tarpanov@inrne.bas.bg

terms. This Hamiltonian is expressed in terms of quasiparticle creation and annihilation operators, $\alpha^{\dagger}_{jm}(\alpha_{jm})$, obtained from the corresponding particle operators through a Bogoliubov transformation.

The quasiparticle separable Hamiltonian is then adopted to solve the QRPA eigenvalue equations to generate QRPA phonon operators of multipolarity $\lambda\mu$

$$Q^{\dagger}_{i\lambda\mu} = \frac{1}{2}\sum_{jj'}\left\{\psi^{i\lambda}_{jj'}[\alpha^{\dagger}_{j}\alpha^{\dagger}_{j'}]_{\lambda\mu} - (-1)^{\lambda-\mu}\varphi^{i\lambda}_{jj'}[\alpha_{j'}\alpha_{j}]_{\lambda-\mu}\right\} \quad (1)$$

and their energies $\omega_{i\lambda}$.

The probability amplitudes $\psi^{i\lambda}_{jj'}$ and $\varphi^{i\lambda}_{jj'}$ fulfill the relations,

$$\frac{1}{2}\sum_{jj'}\left[\psi^{i\lambda}_{jj'}\psi^{i'\lambda}_{jj'} - \varphi^{i\lambda}_{jj'}\varphi^{i'\lambda'}_{jj'}\right] = \delta_{ii'}\delta_{\lambda\lambda'}, \quad (2)$$

resulting from enforcing on the phonon operators the normalization condition

$$\begin{aligned}&\langle 0|Q_{i'\lambda'\mu'}Q^{\dagger}_{i\lambda\mu}|0\rangle = \\ &\langle 0|[Q_{i'\lambda'\mu'}, Q^{\dagger}_{i\lambda\mu}]|0\rangle \simeq \delta_{ii'}\delta_{\lambda\lambda'}\delta_{\mu\mu'}.\end{aligned} \quad (3)$$

The approximate equality follows from replacing the QRPA correlated ground state with the quasiparticle BCS vacuum (quasiboson approximation).

The quasiparticle separable Hamiltonian is then expressed into the phonon form

$$H_{\rm QPM} = \sum_{i\mu}\omega_{i\lambda}Q^{\dagger}_{i\lambda\mu}Q_{i\lambda\mu} + H_{vq}, \quad (4)$$

where the first term is the unperturbed phonon Hamiltonian and H_{vq} is a phonon-coupling piece whose exact expression can be found in Ref. [37].

It is worth pointing out that, among the QRPA phonons, only few are collective, composed of a coherent linear combination of two-quasiparticle configurations. The phonon Hamiltonian is then accordingly diagonalized in a space spanned by states composed of one, two, and three QRPA phonons.

The eigenfunctions have the structure

$$\begin{aligned}&\Psi_{\nu}(JM)\\ &= \sum_{i} R_i(\nu J)Q^{\dagger}_{iJM}|0\rangle + \sum_{\substack{i_1\lambda_1\\ i_2\lambda_2}} P^{i_1\lambda_1}_{i_2\lambda_2}(\nu J)\left[Q^{\dagger}_{i_1\lambda_1}\otimes Q^{\dagger}_{i_2\lambda_2}\right]_{JM}|0\rangle\\ &\quad + \sum_{\substack{i_1\lambda_1 i_2\lambda_2\\ i_3\lambda_3 I}} T^{i_1\lambda_1 i_2\lambda_2 I}_{i_3\lambda_3}(\nu J)\left[\left[Q^{\dagger}_{i_1\lambda_1}\otimes Q^{\dagger}_{i_2\lambda_2}\right]_{I}\otimes Q^{\dagger}_{i_3\lambda_3}\right]_{JM}|0\rangle,\end{aligned} \quad (5)$$

where ν labels the specific QPM excited state of total spin JM. The above wave functions are properly antisymmetrized according to the procedure outlined in [34,37]. Accounting for the Pauli principle is of special importance for a reliable calculation of the $E2$ and $M1$ transition strengths.

Each transition operator is composed of two pieces [38]. The first is linear in the QRPA phonon operators $Q_{i\lambda\mu}$ and $Q^{\dagger}_{i\lambda\mu}$ and, therefore, connects states differing by one phonon. This is the leading term and promotes the *boson allowed* transitions. The second piece links only states with the same number of phonons and promotes the *boson forbidden* transitions. The first term is dominant in the $E2$ transitions. The second is responsible for the $M1$ transitions, which would be forbidden otherwise.

As in our previous investigations [33–36], we used a single particle basis which encompasses all bound states from the bottom of the well up to the quasibound states embedded into the continuum. We adopted for the Woods-Saxon potential the parameters used previously for ^{136}Ba [34], which fit on average the single particle spectra of the $A = 141$ nuclei. Only we increased slightly, by about 300 keV, the energy of the $2d5/2$ with respect to the $1g7/2$ proton orbits in order to weaken the effect of pairing. As we shall see, these changes do not alter the spectrum of ^{136}Ba computed in the previous calculation.

We fit the strength of the quadrupole-quadrupole interaction on the energy and $E2$ decay strength of the 2^+_1 and the coupling constant of the quadrupole pairing on the overall properties of the low-lying 2^+ isovector state. We fixed the other Hamiltonian parameters following the procedure outlined in Ref. [34]. Such a procedure is the one adopted in all QPM calculations [37–39] and is independent of the specific quantities to be computed. In this respect, our QPM calculation is to be considered parameter free.

Because of the large model space, we used effective charges very close to the bare values. More specifically we put $e_p = 1.05$ for protons and $e_n = 0.05$ for neutrons. We also used the spin-gyromagnetic quenching factor $g_s = 0.8$.

III. CALCULATION AND RESULTS

A. QRPA analysis

The first step of our QPM strategy in facing the study of MS states is to ascertain that the low-lying QRPA spectrum contains, in addition to the np symmetric collective 2^+, with n and p amplitudes in phase, another 2^+ state which is fairly collective and is dominantly np nonsymmetric, with neutron and proton amplitudes in opposition of phase. This is a preliminary condition for obtaining a classification of multiphonon states according to the np symmetry. Such a requirement is not at all granted a priori in a microscopic approach.

Some QRPA results are shown in Tables I through III for ^{134}Xe, ^{136}Ba, and ^{138}Ce. In all nuclei, the lowest 2^+_1

TABLE I. Energy and $E2$ decay strengths of the lowest $[2^+]_{\rm RPA}$ states.

Nucleus	λ^{π}_i	$\omega_{\lambda^{\pi}_i}$ (MeV)	$B(E2)\downarrow$ (W.u.)	%EWSR
^{134}Xe	2^+_1	1.02	19.6	4.0
	2^+_2	1.97	1.44	0.6
	2^+_3	2.23	0.0017	0.001
^{136}Ba	2^+_1	1.03	24.8	5.07
	2^+_2	2.12	1.7	0.71
	2^+_3	2.25	0.074	0.033
^{138}Ce	2^+_1	1.02	22.2	4.4
	2^+_2	2.21	1.6	0.7
	2^+_3	2.31	3.96	1.7

TABLE II. Quasiparticle composition of the lowest $[2^+]_{\mathrm{RPA}}$ states in ^{134}Xe, ^{136}Ba, and ^{138}Ce. Only the largest components are given. The states are normalized according to Eq. (2).

Nucleus	State	$(q_1q_2)_n$		$(q_1q_2)_p$	
^{134}Xe	2_1^+	$+0.87(1h_{11/2}\otimes 1h_{11/2})_n$	36.35%	$+0.70(1g_{7/2}\otimes 1g_{7/2})_p$	23.0%
		$+0.44(2d_{3/2}\otimes 2d_{3/2})_n$	9.42%	$+0.20(2d_{5/2}\otimes 2d_{5/2})_p$	1.77%
		$+0.29(2d_{3/2}\otimes 3s_{1/2})_n$	7.95%	$+0.19(1h_{11/2}\otimes 1h_{11/2})_p$	1.60%
				$+0.17(1g_{7/2}\otimes 2d_{3/2})_p$	2.52%
		total	65%	total	35%
	2_2^+	$+0.62(1h_{11/2}\otimes 1h_{11/2})_n$	18.88%	$-1.12(1g_{7/2}\otimes 1g_{7/2})_p$	62.5%
		$+0.49(2d_{3/2}\otimes 2d_{3/2})_n$	11.8%	$-0.11(2d_{5/2}\otimes 2d_{5/2})_p$	0.57%
		$+0.18(2d_{3/2}\otimes 3s_{1/2})_n$	3.1%	$-0.10(1h_{11/2}\otimes 1h_{11/2})_p$	0.5%
		total	35%	total	65%
	2_3^+	$+0.62(1h_{11/2}\otimes 1h_{11/2})_n$	19.1%	$-0.15(1g_{7/2}\otimes 1g_{7/2})_p$	1.1%
		$-1.24(2d_{3/2}\otimes 2d_{3/2})_n$	77.5%		
		$+0.14(2d_{3/2}\otimes 3s_{1/2})_n$	2.0%		
		total	99%	total	1.1%
^{136}Ba	2_1^+	$+0.83(1h_{11/2}\otimes 1h_{11/2})_n$	32.8%	$+0.64(1g_{7/2}\otimes 1g_{7/2})_p$	19.6%
		$+0.43(2d_{3/2}\otimes 2d_{3/2})_n$	8.9%	$+0.29(2d_{5/2}\otimes 2d_{5/2})_p$	3.8%
		$+0.27(2d_{3/2}\otimes 3s_{1/2})_n$	7.1%	$+0.27(1h_{11/2}\otimes 1h_{11/2})_p$	3.4%
				$+0.22(1g_{7/2}\otimes 2d_{3/2})_p$	4.1%
		total	59%	total	41%
	2_2^+	$+0.49(1h_{11/2}\otimes 1h_{11/2})_n$	11.9%	$-0.98(1g_{7/2}\otimes 1g_{7/2})_p$	47.7%
		$+0.82(2d_{3/2}\otimes 2d_{3/2})_n$	33.2%	$-0.17(2d_{5/2}\otimes 2d_{5/2})_p$	1.35%
		$+0.13(2d_{3/2}\otimes 3s_{1/2})_n$	1.7%	$-0.14(1h_{11/2}\otimes 1h_{11/2})_p$	0.9%
		total	48%	total	52%
	2_3^+	$+0.78(1h_{11/2}\otimes 1h_{11/2})_n$	30.7%	$-0.42(1g_{7/2}\otimes 1g_{7/2})_p$	8.8%
		$-1.07(2d_{3/2}\otimes 2d_{3/2})_n$	56.8%		
		$+0.18(2d_{3/2}\otimes 3s_{1/2})_n$	3.1%		
		total	91%	total	9%
^{138}Ce	2_1^+	$+0.92(1h_{11/2}\otimes 1h_{11/2})_n$	40.5%	$+0.43(1g_{7/2}\otimes 1g_{7/2})_p$	8.6%
		$+0.46(2d_{3/2}\otimes 2d_{3/2})_n$	10.51%	$+0.31(2d_{5/2}\otimes 2d_{5/2})_p$	4.21%
		$+0.302(2d_{3/2}\otimes 3s_{1/2})_n$	8.9%	$+0.28(1h_{11/2}\otimes 1h_{11/2})_p$	3.43%
				$+0.21(1g_{7/2}\otimes 2d_{3/2})_p$	3.40%
		total	72%	total	28%
	2_2^+	$+0.16(1h_{11/2}\otimes 1h_{11/2})_n$	1.15%	$+0.44(1g_{7/2}\otimes 1g_{7/2})_p$	9.84%
		$-1.29(2d_{3/2}\otimes 2d_{3/2})_n$	83.0%	$+0.2(2d_{5/2}\otimes 2d_{5/2})_p$	1.99%
		total	85%	total	15%
	2_3^+	$+0.85(1h_{11/2}\otimes 1h_{11/2})_n$	35.92%	$-0.88(1g_{7/2}\otimes 1g_{7/2})_p$	38.9%
		$-0.33(2d_{3/2}\otimes 2d_{3/2})_n$	5.45%	$-0.34(2d_{5/2}\otimes 2d_{5/2})_p$	5.9%
		$+0.18(2d_{3/2}\otimes 3s_{1/2})_n$	3.05%	$-0.23(1h_{11/2}\otimes 1h_{11/2})_p$	2.54%
				$+0.15(1g_{7/2}\otimes 2d_{5/2})_p$	2.23%
		total	46%	total	54%

is by far the most collective quadrupole state (Table I). Table II shows that proton and neutron components are in phase thereby establishing the np symmetric nature of such a state.

The second lowest 2_2^+ in ^{134}Xe and ^{136}Ba is fairly collective (Table I) and has a np MS character, with the main proton and neutron amplitudes in opposition of phase (Table II). In ^{138}Ce, instead, there are two 2^+ states which get an appreciable $E2$ strength (Table I) and have a dominant np MS character (Table II). The third 2_3^+ is more collective and, therefore, is the best candidate for being considered the counterpart of the IBM-2 MS state. In our microscopic analysis, however, both

TABLE III. Energy of the lowest two-quasiparticle proton states.

Nucleus	q_1q_2	$E_{q_1} + E_{q_2}$ [MeV]
^{134}Xe	$(1g_{7/2} \otimes 1g_{7/2})_p$	2.124
	$(1g_{7/2} \otimes 2d_{5/2})_p$	2.943
	$(2d_{5/2} \otimes 2d_{5/2})_p$	3.762
^{136}Ba	$(1g_{7/2} \otimes 1g_{7/2})_p$	2.333
	$(2d_{3/2} \otimes 3s_{1/2})_n$	2.886
	$(2d_{5/2} \otimes 2d_{5/2})_p$	3.440
^{138}Ce	$(1g_{7/2} \otimes 1g_{7/2})_p$	2.627
	$(1g_{7/2} \otimes 2d_{5/2})_p$	2.892
	$(2d_{5/2} \otimes 2d_{5/2})_p$	3.158

2_2^+ and 2_3^+ states play a role and are to be treated on equal footing.

In order to understand why the $E2$ response in ^{138}Ce is different with respect to the other two isotones, it is useful to analyze the energies of the three lowest two-quasiparticle proton states (Table III). The third level in ^{134}Xe and ^{136}Ba is quite high in energy with respect to the other two, while in ^{138}Ce the three levels are closely packed.

This is a clear shell effect. Indeed, in ^{138}Ce the $1g7/2$ proton subshell is filled. Their low-lying excitations are therefore due to the diffuseness of the Fermi surface induced by pairing. As Table II shows clearly, the 2_3 in ^{138}Ce gets contribution from several proton configurations, made accessible by the diffuse Fermi surface. The corresponding state in the other two isotones is noncollective. Since the $1g7/2$ proton subshell is only partially filled, the proton chemical potential is lower than in ^{138}Ce. It follows that the energy difference between the quasiproton levels above and below the subshell gap remains too high (Table III).

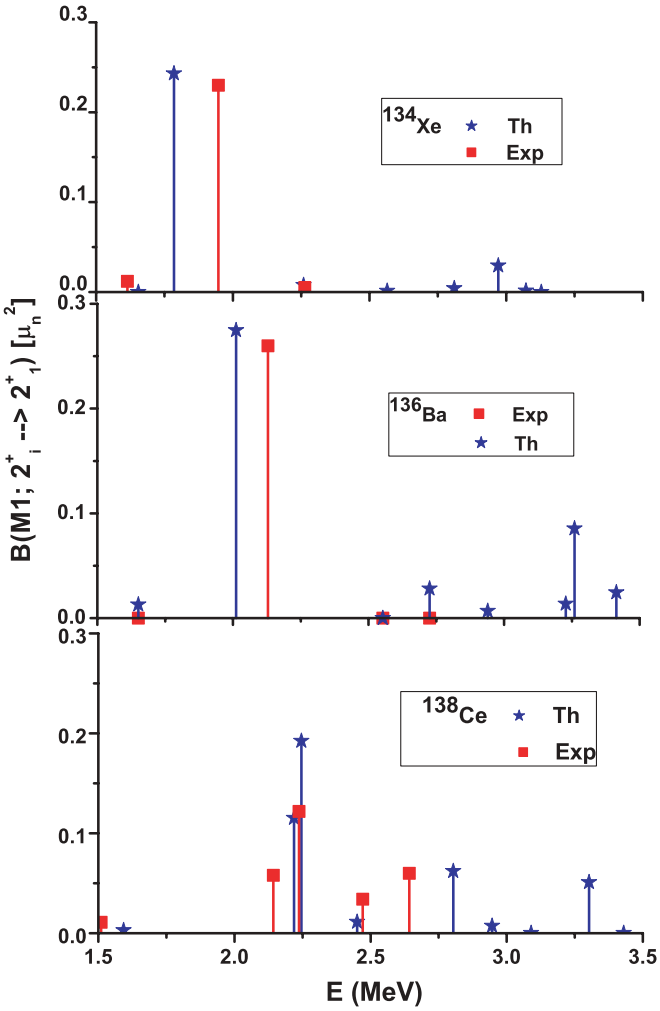

FIG. 1. (Color online) QPM versus Experimental $M1$ strength distribution in ^{134}Xe, ^{136}Ba, and ^{138}Ce.

B. QPM results

Let us now investigate the QPM states (Table IV) and how their phonon composition affects the $E2$ as well as the $M1$ transitions (Table V).

In all three nuclei, the first 2_1^+ is mostly accounted for by the lowest QRPA one-phonon component, although the amplitude of the two-phonon piece is appreciable, especially in ^{136}Ba. The second QPM state has a dominant two-phonon component in all three nuclei.

The other states mark a difference between the ^{138}Ce and the other two isotones ^{134}Xe and ^{136}Ba. In the latter nuclei, the third 2_3^+ is dominated by the np MS QRPA phonon and corresponds to the MS state in IBM-2. In ^{138}Ce, the np MS QRPA phonon is shared by the 2_4^+ and, to a less extent, the 2_3^+. Both QPM states contain the second QRPA $[2_2^+]_{\mathrm{RPA}}$ with an appreciable amplitude. We have pointed out already that in ^{138}Ce the residual quadrupole collectivity was shared by the second and third QRPA 2^+ states.

Apparently, the interaction between these two fairly collective states lead to the generation of two QPM states with np MS character. This is reflected in the $M1$ transitions (Tables V). While in ^{134}Xe and ^{136}Ba we have one strong $M1$ peak (first and second panels of Fig. 1), in ^{138}Ce the $M1$ strength splits into two peaks (third panel of Fig. 1).

Figure 1 shows also that the main $M1$ peaks move upward in energy as the number of valence protons increases. Apparently, because of the gap between $1g7/2$ and the other subshells, the Fermi energy surface gets more and more diffuse until the protons fill the $1g7/2$ shell. In support of such a physical explanation, we have checked that, as the protons increase further in number and start to fill the shell beyond the $1g7/2$ subshell closure, the Fermi surface gets less diffuse and brings the excited states back to lower energies. This feature emphasizes once more the role of the shell structure in determining the properties of the low-lying states in open shell nuclei.

The agreement between the QPM calculation and experiments is good for both $M1$ and $E2$ strength distributions, on quantitative and qualitative ground (Figs. 1 and 2). In particular, the selection rules which provide the signature for the np symmetry nature of the 2^+ states are fulfilled with high accuracy.

TABLE IV. Energy and structure of selected low-lying excited states. Only the dominant components are presented. The mixed symmetry $2^+_{\rm MS}$ in ^{136}Ba is the QPM 2^+_3 but corresponds to the measured 2^+_4.

Nucleus	State J^π	E (keV)		Phonon structure,%
		EXP	QPM	
^{134}Xe	2^+_1	847	906	$89\%[2^+_1]_{\rm RPA} + 8\%[2^+_1 \otimes 2^+_1]_{\rm RPA}$
	2^+_2	1614	1654	$54\%[2^+_1 \otimes 2^+_1]_{\rm RPA} + 8\%[2^+_1]_{\rm RPA} + 10\%[2^+_2]_{\rm RPA} + 10\%[2^+_3]_{\rm RPA} + 13\%[2^+_4]_{\rm RPA}$
	2^+_3	1947	1787	$75\%[2^+_2]_{\rm RPA}$
	2^+_4	2263	2259	$64\%[2^+_3]_{\rm RPA} + 19\%[2^+_3]_{\rm RPA} + 6\%[2^+_1 \otimes 2^+_1]_{\rm RPA}$
^{136}Ba	2^+_1	810	789	$78\%[2^+_1]_{\rm RPA} + 15\%[2^+_1 \otimes 2^+_1]_{\rm RPA}$
	2^+_2	1551	1651	$46\%[2^+_1 \otimes 2^+_1]_{\rm RPA} + 16\%[2^+_1]_{\rm RPA}$
	$2^+_{\rm MS}$	2129	2012	$60\%[2^+_2]_{\rm RPA} + 25\%[2^+_3]_{\rm RPA}$
^{138}Ce	2^+_1	788	808	$85\%[2^+_1]_{\rm RPA} + 7.3\%[2^+_1 \otimes 2^+_1]_{\rm RPA}$
	2^+_2	1510	1593	$54\%[2^+_1 \otimes 2^+_1]_{\rm RPA} + 6.3\%[2^+_1]_{\rm RPA} + 20\%[2^+_2]_{\rm RPA}$
	2^+_3	2143	2219	$5.0\%[2^+_2]_{\rm RPA} + 40\%[2^+_3]_{\rm RPA} + 12\%[2^+_1 \otimes 2^+_1]_{\rm RPA}$
	2^+_4	2237	2457	$71\%[2^+_3]_{\rm RPA} + 11\%[2^+_2]_{\rm RPA} + 1\%[2^+_1 \otimes 2^+_1]_{\rm RPA}$
	2^+_5	2471	2450	$20\%[2^+_4]_{\rm RPA} + 14\%[2^+_1 \otimes 2^+_2]_{\rm RPA} + 43\%[2^+_1 \otimes 2^+_1 \otimes 2^+_1]_{\rm RPA}$
	2^+_6	2642	2804	$98\%[2^+_5]_{\rm RPA}$

TABLE V. QPM versus experimental strengths of $E2$ and $M1$ transitions. The $E2$ strengths are given in W.u. for ^{134}Xe and ^{138}Ce, and in e^2b^2 for ^{136}Ba. The $M1$ strengths are in μ_N^2. The $2^+_{\rm MS}$ in ^{136}Ba is the QPM 2^+_3 but corresponds to the measured 2^+_4.

Nucleus	$J_i \to J_f$	B(E2)		B(M1)	
		EXP	QPM	EXP	QPM
^{134}Xe	$2^+_1 \to 0^+_{gs}$	15.3(11)	14.0		
	$2^+_2 \to 0^+_{gs}$	0.63(4)	0.5		
	$2^+_3 \to 0^+_{gs}$	0.58(3)	2.3		
	$2^+_4 \to 0^+_{gs}$	0.25(2)	0.04		
	$2^+_2 \to 2^+_1$	18(2)	22	0.012(3)	1.0×10^{-6}
	$2^+_3 \to 2^+_1$	0.43(12)	1.7	0.23(1)	0.24
	$2^+_4 \to 2^+_1$	2.2(2)	3.0	0.005(2)	0.008
^{136}Ba	$0^+_{gs} \to 2^+_1$	0.400(5)	0.33		
	$0^+_{gs} \to 2^+_2$	0.016(4)	0.046		
	$0^+_{gs} \to 2^+_{\rm MS}$	0.045(5)	0.065		
	$2^+_2 \to 2^+_1$	0.09(4)	0.12		
	$2^+_{\rm MS} \to 2^+_1$			0.26(3)	0.27
	$0^+_{gs} \to 1^+_1$			0.13(2)	0.15
^{138}Ce	$2^+_1 \to 0^+_{gs}$	21.2(14)	19		
	$2^+_2 \to 0^+_{gs}$	1.16(8)	0.45		
	$2^+_3 \to 0^+_{gs}$		3.4		
	$2^+_4 \to 0^+_{gs}$	1.86(16)	2.0		
	$2^+_5 \to 0^+_{gs}$	0.74(20)	0.14		
	$2^+_4 \to 0^+_{gs}$	0.42(8)	0.72		
	$2^+_2 \to 2^+_1$	28(2)	26	0.011(2)	0.003
	$2^+_3 \to 2^+_1$		6.1	0.058(6)	0.11
	$2^+_4 \to 2^+_1$	0.65(10)	0.28	0.122(10)	0.19
	$2^+_5 \to 2^+_1$			$\leqslant$0.034(3)	0.011
	$2^+_6 \to 2^+_1$			$\leqslant$0.069(47)	0.062

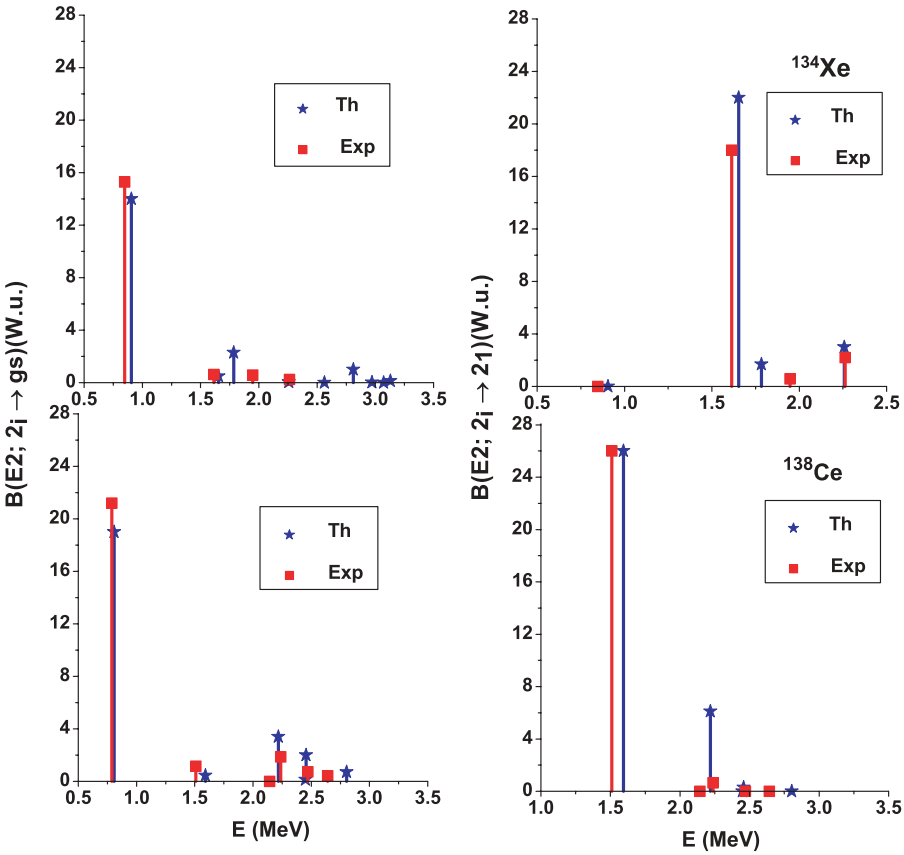

FIG. 2. (Color online) QPM $E2$ strength distribution in ^{134}Xe and ^{138}Ce. ^{136}Ba has a similar behavior (see Table III).

IV. CONCLUDING REMARKS

The QPM investigation presented here has shown that the low-lying states observed in the $N = 80$ isotones can be well classified according to the np symmetry in agreement with the F-spin IBM-2 scheme. The splitting of the $M1$ strength observed in ^{138}Ce is shown to be due to the specific shell structure of this nucleus. Because of the proton $1g7/2$ subshell closure, the low-lying proton excitations are made possible by the diffuse Fermi surface induced by pairing. This yields a relatively higher density of two-quasiparticle states at low energy which leads to a higher number of low-lying states with MS character, hence, the splitting of the $M1$ strength. This is a genuine shell effect which can be explained only within a microscopic context.

ACKNOWLEDGMENTS

The present work was partly supported by the Italian Ministry of Instruction, University, and Research (MIUR) and by the Bulgarian Science Foundation (contract nos. VUF06/05 and DAAD-09). Ch.S. thanks the INFN for Financial support and hospitality. It is a pleasure to thank N. Pietralla and T. Ahn for useful discussions and for having permitted the use of the data on ^{134}Xe before their publication.

[1] F. Iachello and A. Arima, *The Interacting Boson Model* (Cambridge University Press, Cambridge, U.K., 1987).
[2] A. Arima, T. Otsuka, F. Iachello, and I. Talmi, Phys. Lett. **B66**, 205 (1977).
[3] T. Otsuka, A. Arima, and F. Iachello, Nucl. Phys. **A309**, 1 (1978).
[4] F. Iachello, Phys. Rev. Lett. **53**, 1427 (1984).
[5] A. Bohr and B. Mottelson, *Nuclear Structure*, Vol. 2 (Benjamin, Reading, Massachusetts, 1975).
[6] N. Lo Iudice and F. Palumbo, Phys. Rev. Lett. **41**, 1532 (1978).
[7] D. Bohle, A. Richter, W. Steffen, A. E. L. Dieperink, N. Lo Iudice, F. Palumbo, and O. Scholten, Phys. Lett. **B137**, 27 (1984).
[8] A. Richter, Prog. Part. Nucl. Phys. **34**, 261 (1995).
[9] U. Kneissl, H. H. Pitz, and A. Zilges, Prog. Part. Nucl. Phys. **37**, 349 (1996).
[10] N. Lo Iudice, Rivista Nuovo Cimento **23**, n. 9, 1 (2000).
[11] N. Pietralla, P. von Brentano, and A. F. Lisetskiy, Prog. Part. Nucl. Phys. **60**, 225 (2008).
[12] K. P. Lieb, H. G. Börner, M. S. Dewey, J. Jolie, S. J. Robinson, S. Ulbig, and Ch. Winter, Phys. Lett. **B215**, 50 (1988).
[13] H. Nakada, T. Otsuka, and T. Sebe, Phys. Rev. Lett. **67**, 1086 (1991).
[14] N. Pietralla, C. Fransen, D. Belic, P. von Brentano, C. Friessner, U. Kneissl, A. Linnemann, A. Nord, H. H. Pitz, T. Otsuka, I. Schneider, V. Werner, and I. Wiedenhover, Phys. Rev. Lett. **83**, 1303 (1999).

[15] N. Pietralla, C. Fransen, P. von Brentano, A. Dewald, A. Fitzler, C. Friessner, and J. Gableske, Phys. Rev. Lett. **84**, 3775 (2000).
[16] C. Fransen, N. Pietralla, P. von Brentano, A. Dewald, J. Gableske, A. Gade, A. F. Lisetskiy, and V. Werner, Phys. Lett. **B508**, 219 (2001).
[17] C. Fransen, N. Pietralla, Z. Ammar, D. Bandyopadhyay, N. Boukharouba, P. von Brentano, A. Dewald, J. Gableske, A. Gade, J. Jolie, U. Kneissl, S. R. Lesher, A. F. Lisetskiy, M. T. McEllistrem, M. Merrick, H. H. Pitz, N. Warr, V. Werner, and S. W. Yates, Phys. Rev. C **67**, 024307 (2003).
[18] O. Burda, N. Botha, J. Carter, R. W. Fearick, S. V. Förtsch, C. Fransen, H. Fujita, J. D. Holt, M. Kuhar, A. Lenhardt, P. von Neumann-Cosel, R. Neveling, N. Pietralla, V. Yu. Ponomarev, A. Richter, O. Scholten, E. Sideras-Haddad, F. D. Smit, and J. Wambach, Phys. Rev. Lett. **99**, 092503 (2007).
[19] N. Pietralla, C. J. Barton, R. Krücken, C. W. Beausang, M. A. Caprio, R. F. Casten, J. R. Cooper, A. A. Hecht, H. Newman, J. R. Novak, and N. V. Zamfir, Phys. Rev. C **64**, 031301(R) (2001).
[20] V. Werner, D. Belic, P. von Brentano, C. Fransen, A. Gade, H. von Garrel, J. Jolie, U. Kneissl, C. Kostall, A. Linnemann, A. F. Lisetskiy, N. Pietralla, H. H. Pitz, M. Scheck, K.-H. Speidel, F. Stedile, and S. W. Yates, Phys. Lett. **B550**, 140 (2002).
[21] C. Fransen, N. Pietralla, A. P. Tonchev, M. W. Ahmed, J. Chen, G. Feldman, U. Kneissl, J. Li, V. Litvinenko, B. Perdue, I. V. Pinayev, H.-H. Pitz, R. Prior, K. Sabourov, M. Spraker, W. Tornow, H. R. Weller, V. Werner, Y. K. Wu, and S. W. Yates, Phys. Rev. C **70**, 044317 (2004).
[22] C. Fransen, V. Werner, D. Bandyopadhyay, N. Boukharouba, S. R. Lesher, M. T. McEllistrem, J. Jolie, N. Pietralla, P. von Brentano, and S. W. Yates, Phys. Rev. C **71**, 054304 (2005).
[23] E. Elhami, J. N. Orce, S. Mukhopadhyay, S. N. Choudry, M. Scheck, M. T. McEllistrem, and S. W. Yates, Phys. Rev. C **75**, 011301(R) (2007).
[24] S. R. Lesher, C. J. McKay, M. Mynk, D. Bandyopadhyay, N. Boukharouba, C. Fransen, J. N. Orce, M. T. McEllistrem, and S. W. Yates, Phys. Rev. C **75**, 034318 (2007).
[25] D. Bandyopadhyay, S. R. Lesher, C. Fransen, N. Boukharouba, P. E. Garrett, K. L. Green, M. T. McEllistrem, and S. W. Yates, Phys. Rev. C **76**, 054308 (2007).
[26] N. Pietralla, C. Fransen, A. Gade, N. A. Smirnova, P. von Brentano, V. Werner, and S. W. Yates, Phys. Rev. C **68**, 031305(R) (2003).
[27] H. Klein, A. F. Lisetskiy, N. Pietralla, C. Fransen, A. Gade, and P. von Brentano, Phys. Rev. C **65**, 044315 (2002).
[28] N. Pietralla, D. Belic, P. von Brentano, C. Fransen, R.-D. Herzberg, U. Kneissl, H. Maser, P. Matschinsky, A. Nord, T. Otsuka, H. H. Pitz, V. Werner, and I. Wiedenhover, Phys. Rev. C **58**, 796 (1998).
[29] G. Rainovski, N. Pietralla, T. Ahn, C. J. Lister, R. V. F. Janssens, M. P. Carpenter, S. Zhu, and C. J. Barton III, Phys. Rev. Lett. **96**, 122501 (2006).
[30] T. Ahn, N. Pietralla, G. Rainovski, A. Costin, K. Dusling, T. C. Li, A. Linnemann, and S. Pontillo, Phys. Rev. C **75**, 014313 (2007).
[31] T. Ahn and N. Pietralla (private communication).
[32] A. F. Lisetskiy, N. Pietralla, C. Fransen, R. V. Jolos, and P. von Brentano, Nucl. Phys. **A677**, 1000 (2000).
[33] N. Lo Iudice and Ch. Stoyanov, Phys. Rev. C **62**, 047302 (2000).
[34] N. Lo Iudice and Ch. Stoyanov, Phys. Rev. C **65**, 064304 (2002).
[35] N. Lo Iudice and Ch. Stoyanov, Phys. Rev. C **69**, 044312 (2004).
[36] N. Lo Iudice and Ch. Stoyanov, Phys. Rev. C **73**, 037305 (2006).
[37] V. G. Soloviev, *Theory of Atomic Nuclei: Quasiparticles and Phonons* (Institute of Physics Publishing, Bristol, 1992).
[38] V. Yu. Ponomarev, Ch. Stoyanov, N. Tsoneva, and M. Grinberg, Nucl. Phys. **A635**, 470 (1998).
[39] M. Grinberg, Ch. Stoyanov, and N. Tsoneva, Phys. Part. Nuclei **29**, 606 (1998).